Parameterization of the Vertical Velocity Equation for Shallow Cumulus Clouds

Stephan R. de Roode

Department of Multi-Scale Physics, TU Delft, Delft, Netherlands

A. Pier Siebesma

Department of Multi-Scale Physics, TU Delft, Delft, and KNMI, De Bilt, Netherlands

Harm J. J. Jonker and Yoerik de Voogd

Department of Multi-Scale Physics, TU Delft, Delft, Netherlands

ABSTRACT

The application of a steady-state vertical velocity equation for parameterized moist convective updrafts in climate and weather prediction models is currently common practice. This equation usually contains an advection, a buoyancy, and a lateral entrainment term, whereas the effects of pressure gradient and subplume contributions are typically incorporated as proportionality constants a and b for the buoyancy and the entrainment terms, respectively. A summary of proposed values of these proportionality constants a and b in the literature demonstrates that there is a large uncertainty in their most appropriate values. To shed new light on this situation an analysis is presented of the full vertical budget equation for shallow cumulus clouds obtained from large eddy simulations of three different Global Energy and Water Cycle Experiment (GEWEX) Cloud System Study (GCSS) intercomparison cases. It is found that the pressure gradient term is the dominant sink term in the vertical velocity budget, whereas the entrainment term only gives a small contribution. This result is at odds with the parameterized vertical velocity equation in the literature as it employs the entrainment term as the major sink term. As a practical solution the damping effect of the pressure term may be parameterized in terms of the lateral entrainment rates as used for thermodynamic quantities like the total specific humidity. By using a least squares method, case-dependent optimal values are obtained for the proportionality constants a and b, which are linearly related with each other. This relation can be explained from a linear relationship between the lateral entrainment rate and the buoyancy.

1. Introduction

Parameterization schemes of vertical transport of heat, moisture, and momentum by shallow cumulus convection in climate and numerical weather prediction models are often based on the mass flux concept. This approach assumes that the convective transport is well represented by active updrafts driven by condensational heating in the cumulus clouds and passive subsiding motion in the environment. In its simplest form, the updraft properties are described by an entraining plume model whereas the vertical profile of the mass flux follows from the conservation equation for mass as a balance between the entrainment and detrainment rates. The system must be closed by specifying the mass flux at some level, traditionally at cloud base, which has been shown to be intimately connected to the turbulence intensity in the subcloud layer (Grant 2001). Early mass flux schemes did not employ a vertical velocity equation for the convective updrafts (Arakawa and Schubert 1974). In fact, in these schemes cloud-top height is simply diagnosed as the zero buoyancy level where overshoot is taken into account by assuming that a fixed prescribed fraction of the mass flux can reach the next model level (Tiedtke 1989). Such an assumption is rather ad hoc and also introduces an unwanted dependency on the used vertical resolution. Partly as a response to this situation, more recent mass flux schemes are using a vertical velocity equation for the cloudy updrafts (see Table 1 for

Corresponding author address: S. R. de Roode, Department of Multi-Scale Physics, Faculty of Applied Sciences, Lorentzweg 1, 2628 CJ Delft, Netherlands.
E-mail: s.r.deroode@tudelft.nl

TABLE 1. Overview of values used for the constants a and b in the parameterized vertical velocity Eq. (1). The second column gives the acronym used in this paper. The third column shows the equation number of the vertical velocity equation as presented in the original paper. If this equation is different from Eq. (1) it is presented in the last column.

Reference	Acronym	Equation	a	b	Remarks
Simpson and Wiggert (1969)		(1)	$\frac{2}{3}$		$\frac{1}{2}\frac{\partial w_c^2}{\partial z} = aB_c - 0.18\frac{w_c^2}{R}$, where R is cloud radius
Bechtold et al. (2001)	BBGMR	(12)	$\frac{2}{3}$	1	
Gregory (2001)	G01	(11)	$\frac{1}{6}$	1	$\frac{1}{2}\frac{\partial w_c^2}{\partial z} = aB_c - (b'\delta + b\epsilon)w_c^2, b' = \frac{1}{2}$
Von Salzen and McFarlane (2002)	SF	(29)	$\frac{1}{6}$	1	
Jakob and Siebesma (2003)	JS	(7)	$\frac{1}{3}$	2	
Bretherton et al. (2004)	BMG	(17)	1	2	
Cheinet (2004)	C04	(1)	1	1	
Soares et al. (2004)	SMST	(6)	2	1	
Rio and Hourdin (2008)	RH	(5)	1	1	$\frac{\partial \sigma w_c^2}{\partial z} = a\sigma B_c - b'\delta\sigma w_c^2, b' = \frac{1}{2}$ b value found after substitution of Eq. (4)
Neggers et al. (2009)	NKB	(12)	1	$\frac{1}{2}$	$\frac{1}{2}(1-2\mu)\frac{\partial w_c^2}{\partial z} = aB_c - b\epsilon w_c^2, \mu = 0.15$
Pergaud et al. (2009)	PMMC	(7)	1	1	
Rio et al. (2010)	RHCJ	(9)	$\frac{2}{3}$	1	$\frac{1}{2}\frac{\partial w_c^2}{\partial z} = aB_c - (b' + b\epsilon)w_c^2, b' = 0.002$
De Rooy and Siebesma (2010)	RS	(27)	0.62	1	
ECMWF (2010)	ECMWF	(6.9)	$\frac{1}{3}$	1.95	
Kim and Kang (2011)	KK	(11)	$\frac{1}{6}$	2	$\frac{1}{2}\frac{\partial w_c^2}{\partial z} = a(1 - C_\epsilon b)B_c, C_\epsilon = 1/\overline{RH} - 1$

references). One obvious advantage is that cloud-top height can be more realistically estimated by the height at which the in-cloud vertical velocity vanishes. In this way the capability of the moist convective updrafts to penetrate into the inversion can be determined by the kinetic energy gained in the conditionally unstable layer as measured by the vertical velocity. Another advantage is that the vertical velocity equation can also be applied to dry thermals in the subcloud layer in order to determine whether these thermals can reach the level of free convection so that it serves as a realistic and sound alternative for the trigger function for moist convection (Jakob and Siebesma 2003). This has allowed the design of unifying parameterization schemes of convective transport in the dry boundary layer, the subcloud layer, and the cloud layer, such as for instance eddy diffusivity mass flux (EDMF) schemes (Siebesma et al. 2007). A further advantage of the use of a vertical velocity equation is that it can be used to directly estimate the mass flux provided that the fractional area at which the convection occurs is known. This is a very attractive strategy since it is no longer necessary to estimate a detrainment rate in order to derive the mass flux (Neggers et al. 2009). Finally the use of the vertical velocity in convection parameterizations has gained interest also because it allows a link to the microphysical processes that are sensitive to

the vertical velocity such as activation of cloud condensation nuclei (Golaz et al. 2011).

Despite the increased popularity and relevance of the vertical velocity equation in convection parameterizations, there has been little attention to the question of what is the most appropriate parameterized equation for the in-cloud vertical velocity. In fact, inspired by Simpson and Wiggert (1969), who studied the vertical acceleration of a cumulus tower resulting from the difference between the buoyancy and a parameterized drag term, most moist convection schemes use a vertical velocity equation in which the in-cloud vertical velocity w_c is controlled by the in-cloud buoyancy excess with respect to the environment of the cloud B_c, and a sink term that is often taken proportionally to the fractional entrainment rate ϵ:

$$\frac{1}{2}\frac{\partial w_c^2}{\partial z} = aB_c - b\epsilon w_c^2, \tag{1}$$

where z denotes the height. The effects of nonhydrostatic pressure perturbations and subplume fluctuations are believed to be taken into account by a reduction of the buoyancy term ($a < 1$) and by a lateral entrainment term multiplied by a proportionality factor b. The most appropriate formulation, however, is uncertain (Bretherton et al. 2004). Indeed, as can be seen in Table 1 a common

feature of the current in-cloud vertical velocity parameterizations is that they all use different values for the parameterization coefficients a and b.

The purpose of this study is to quantify the contribution of the pressure and subplume terms to the in-cloud vertical velocity budget by using results obtained with a large-eddy simulation (LES) model. Because we will study the full conditionally sampled vertical velocity equation, we can determine their correlation with the buoyancy and entrainment terms and establish the most suitable values for the parameterization coefficients a and b. We will specifically consider LES results of the Barbados Oceanographic and Meteorological Experiment (BOMEX) (Siebesma et al. 2003), the Atmospheric Radiation Measurement (ARM) Program (Brown et al. 2002), and the Rain in Cumulus over the Ocean Experiment (RICO) shallow cumulus model intercomparison studies (VanZanten et al. 2011).

2. The in-cloud vertical velocity equation

Here we will demonstrate that the parameterized vertical velocity Eq. (1) is a simplified form of the full in-cloud conditionally sampled vertical velocity equation. Siebesma and Cuijpers (1995) presented the budget equation for an arbitrary quantity ψ in the mass flux approach:

$$\rho \frac{\partial \sigma \psi_c}{\partial t} = -\frac{\partial \rho \sigma w_c \psi_c}{\partial z} + E_\psi \psi_e - D_\psi \psi_c$$
$$- \frac{\partial \rho \sigma \overline{w'' \psi''}^c}{\partial z} + \rho \sigma [S_\psi]_c, \quad (2)$$

where ρ denotes the density of air, σ the cloud area fraction, t the time, $\overline{w'' \psi''}^c$ describes the vertical flux due to in-cloud subplume fluctuations, and E_ψ and D_ψ are the lateral entrainment and detrainment rates, respectively. The term $[S_\psi]_c$ includes the conditionally sampled contribution of source terms to the in-cloud tendency for ψ_c, which for the vertical velocity includes the buoyancy, the vertical gradient of the pressure, and the Coriolis term:

$$\frac{\partial \sigma w_c}{\partial t} = -\frac{\partial \sigma w_c w_c}{\partial z} - \frac{\partial \sigma \overline{w'' w''}^c}{\partial z} + \frac{E_w}{\rho} w_e - \frac{D_w}{\rho} w_c$$
$$+ \sigma B_c - \sigma \left[\frac{\partial p}{\partial z}\right]_c + 2\Omega \cos\varphi \sigma u_c, \quad (3)$$

with $B_c = (g/\theta_0)(\theta_{v,c} - \overline{\theta_v})$ the in-cloud buoyancy, g is the acceleration due to gravity, θ_v is the virtual potential temperature, θ_0 a reference temperature, Ω is the angular velocity of the earth, φ the latitude, and we use $u_i = (u, v, w)$ to indicate the three components of the wind velocity vector in the $x_i = (x, y, z)$ directions. The definition of the pressure p is given in the appendix. The

subscript "e" is used to indicate the mean value of a quantity in the environment of the cloud. Note that in the spirit of the Boussinesq approximation we neglect the variation of the density with height.

We are well aware of recent developments of a more direct measure of the entrainment rate such as those proposed by Romps (2010) and Dawe and Austin (2011b) that give rise to substantially higher values. We deliberately use here implicitly the more traditional bulk definition of the entrainment and detrainment rates in Eq. (3) since these are compatible with the plume models that are used in the parameterizations, which are the subject of the present analysis. If we compare Eq. (3) to the parameterized vertical velocity Eq. (1), we see that the latter does not include a detrainment term. To get Eq. (3) into a form that is more similar to Eq. (1), we will assume that the mean subsiding motion is zero, $\overline{w} = \sigma w_c + (1 - \sigma)w_e = 0$, and the detrainment term can be eliminated from Eq. (3) with aid of the equation for the mass flux $M_c \equiv \rho \sigma w_c$:

$$\rho \frac{\partial \sigma}{\partial t} = -\frac{\partial M_c}{\partial z} + E_w - D_w, \quad (4)$$

to arrive at

$$\frac{\partial w_c}{\partial t} = \underbrace{B_c}_{\text{Buo}} - \underbrace{\frac{1}{2}\frac{\partial w_c^2}{\partial z}}_{\text{Adv}} - \underbrace{\frac{\epsilon_w w_c^2}{1 - \sigma}}_{\text{Ent}}$$
$$\underbrace{}_{\text{Tend}}$$
$$- \underbrace{\frac{1}{\sigma}\frac{\partial \sigma \overline{w'' w''}^c}{\partial z}}_{\text{Subplume}} - \underbrace{\left[\frac{\partial p}{\partial z}\right]_c}_{\text{Pres}} + \underbrace{2\Omega \cos\varphi u_c}_{\text{Cor}}, \quad (5)$$

where we have made use of the definition of the fractional entrainment rate ϵ_w:

$$E_w \equiv \epsilon_w M_c = \epsilon_w \rho \sigma w_c. \quad (6)$$

A comparison of the steady-state parameterized vertical velocity Eqs. (1) to (5) shows that the subplume and pressure terms are in some way absorbed in the coefficients a and b. Furthermore, the entrainment term in Eq. (5) is divided by the area fraction of the environment $(1 - \sigma)$. Because in shallow cumulus clouds σ is typically less than 0.1, the negligence of the term $(1 - \sigma)$ in the entrainment term in Eq. (1) seems a justifiable approximation. The effect of the Coriolis term is typically neglected.

3. LES results of the in-cloud vertical velocity budget

a. Description of the LES model and the case studies

Results obtained with the Dutch Atmospheric Large Eddy Simulation (DALES) model (Heus et al. 2010)
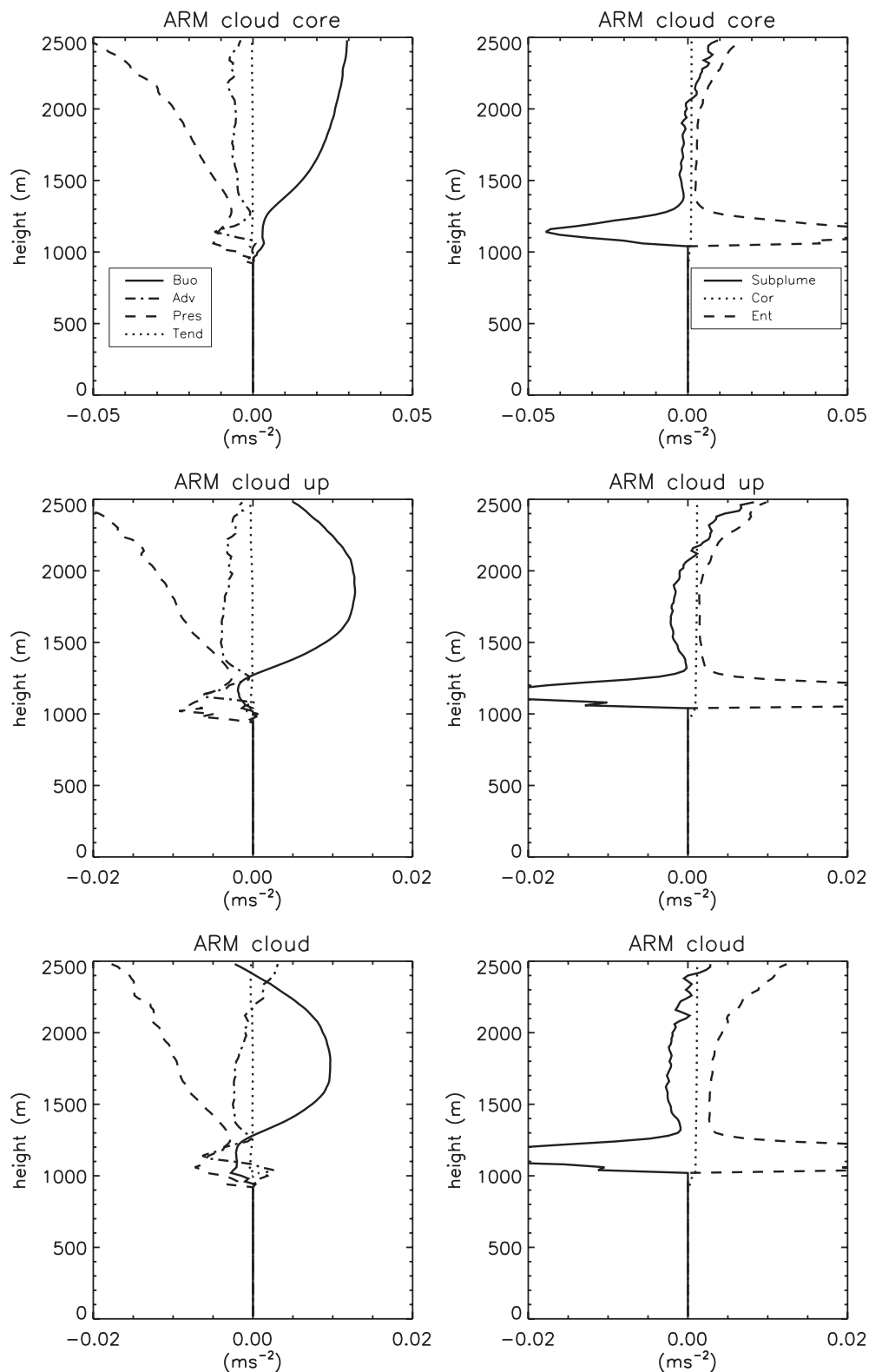
FIG. 1. Hourly-mean in-cloud vertical velocity budgets according to Eq. (5) as obtained from the 10th hour of the ARM simulation for the (top) cloud core, (middle) cloud updraft, and (bottom) cloud decomposition. Line styles as indicated in the legend.

have been used to calculate all the terms in Eq. (5). All the terms in the vertical velocity budget were calculated directly from the LES fields, except for the entrainment term, which was obtained from the residual. The latter term was found to be in a good agreement with a direct calculation of the lateral entrainment term according to Eq. (A9) presented in the appendix. The model has been used to simulate three shallow cumulus cases that were based on data from field campaigns and have been the subject of Global Energy and Water Cycle Experiment (GEWEX) Cloud System Studies (GCCS) intercomparison studies for LES codes and for single-column model versions of GCMs. The large-scale forcings of the BOMEX (Siebesma et al. 2003) and RICO (VanZanten et al. 2011) cases are such that the cumulus cloud fields reach a steady state, whereas the ARM continental cumulus case is driven by time-dependent surface fluxes (Brown et al. 2002). The formation of precipitation is neglected. The simulations lasted 8, 13, and 18 h for the BOMEX, ARM, and RICO cases, respectively, and the results during the spinup phase (first two hours) are omitted.

A horizontal numerical domain size of 12.8×12.8 km^2 was used with 512 grid points in each horizontal direction, and at least 224 vertical levels were used in the vertical direction with a vertical grid size of 12.5 m for BOMEX and RICO and 20 m for ARM. A second-order advection scheme was used, and the subgrid eddy diffusivities were calculated by means of a prognostic subgrid turbulent kinetic energy (TKE) scheme. Every 60 s quantities from the conditionally sampled vertical velocity Eq. (5) were diagnosed, and 10-min averages were stored.

b. LES results

Figure 1 presents the in-cloud vertical velocity budget for three different sampling criteria applied to the ARM data: "cloud sampling" refers to all grid points that contain liquid water, "cloud updraft" to all cloud grid points that are in a updraft, and "cloud core" refers to cloud updraft grid points that are also positively buoyant. Table 2 summarizes the definitions of the terms in the conditionally sampled vertical velocity equation and displayed in the legend of the figures. For convenience we already note that the lateral entrainment term does not act as a sink term. Since the cloud core sampling selects positively buoyant cloud parcels it has the largest buoyancy forcing, in contrast to the cloud sampling criterion, which also includes negatively buoyant cloud parcels and cloudy downdrafts. The vertical velocity budgets, however, do appear qualitatively similar irrespective of the used sampling criterion in the sense that the pressure gradient is the dominant term balancing the buoyancy production.

TABLE 2. Definition of the terms in the conditionally sampled vertical velocity equation according to Eq. (5).

Name	Abbreviation	Term
Tendency	Tend	$\dfrac{\partial w_c}{\partial t}$
Buoyancy	Buo	$B_c = \dfrac{g}{\theta_0}(\theta_{v,c} - \overline{\theta_v})$
Advection	Adv	$-\dfrac{1}{2}\dfrac{\partial w_c^2}{\partial z}$
Entrainment	Ent	$-\dfrac{\epsilon_w w_c^2}{1-\sigma}$
Subplume	Subplume	$-\dfrac{1}{\sigma}\dfrac{\partial \sigma \overline{w''w''}^c}{\partial z}$
Pressure	Pres	$-\left[\dfrac{\partial p}{\partial z}\right]_c$
Coriolis	Cor	$2\Omega \cos\varphi u_c$

We now refine our analysis by considering the vertical velocity budgets for cloud updrafts only, as the cloud core decomposition does not allow for overshooting and because the cloud updraft gives more robust mass flux statistics than the cloud sampling criterion (Siebesma and Cuijpers 1995). Figure 2 displays the cloud updraft budgets for the BOMEX and RICO cases. It can be seen that also for these cases the pressure term is the dominant term that counteracts the buoyancy forcing. The advection term is relatively small compared to the buoyancy forcing. This suggests that only a small fraction of the convective available potential energy (CAPE) is converted into turbulent kinetic energy. Simpson and Wiggert (1969) suggest that the subplume term acts to reduce the buoyancy. The LES results indicate that it is in general a small term except for the levels just above the cloud base where the cloud fraction σ rapidly increases from zero to its maximum value.

The entrainment term exhibits exceptional behavior, as it is found to be small but positive. This implies a negative entrainment rate: $\epsilon_w < 0$. An inspection of the terms presented in the appendix in Eq. (A7) defining the net lateral mixing reveals that the Leibniz terms (see appendix) can have a significant magnitude. This tends to violate the main, implicit assumption that the lateral mixing term is dominated by the resolved horizontal advection term. In addition, the entrainment–detrainment concept to parameterize the horizontal flux divergence assumes that air with average properties of the environment are mixed into the cloud and vice versa. This works well for conserved thermodynamic quantities, but because the vertical velocity near the edge of a cloud shows more complex behavior because of a local evaporative cooling and the subsequent formation of negatively buoyant downdrafts (Heus and Jonker 2008; Jonker et al. 2008; Dawe and Austin 2011a), the lateral entrainment and detrainment rates for the vertical velocity are less
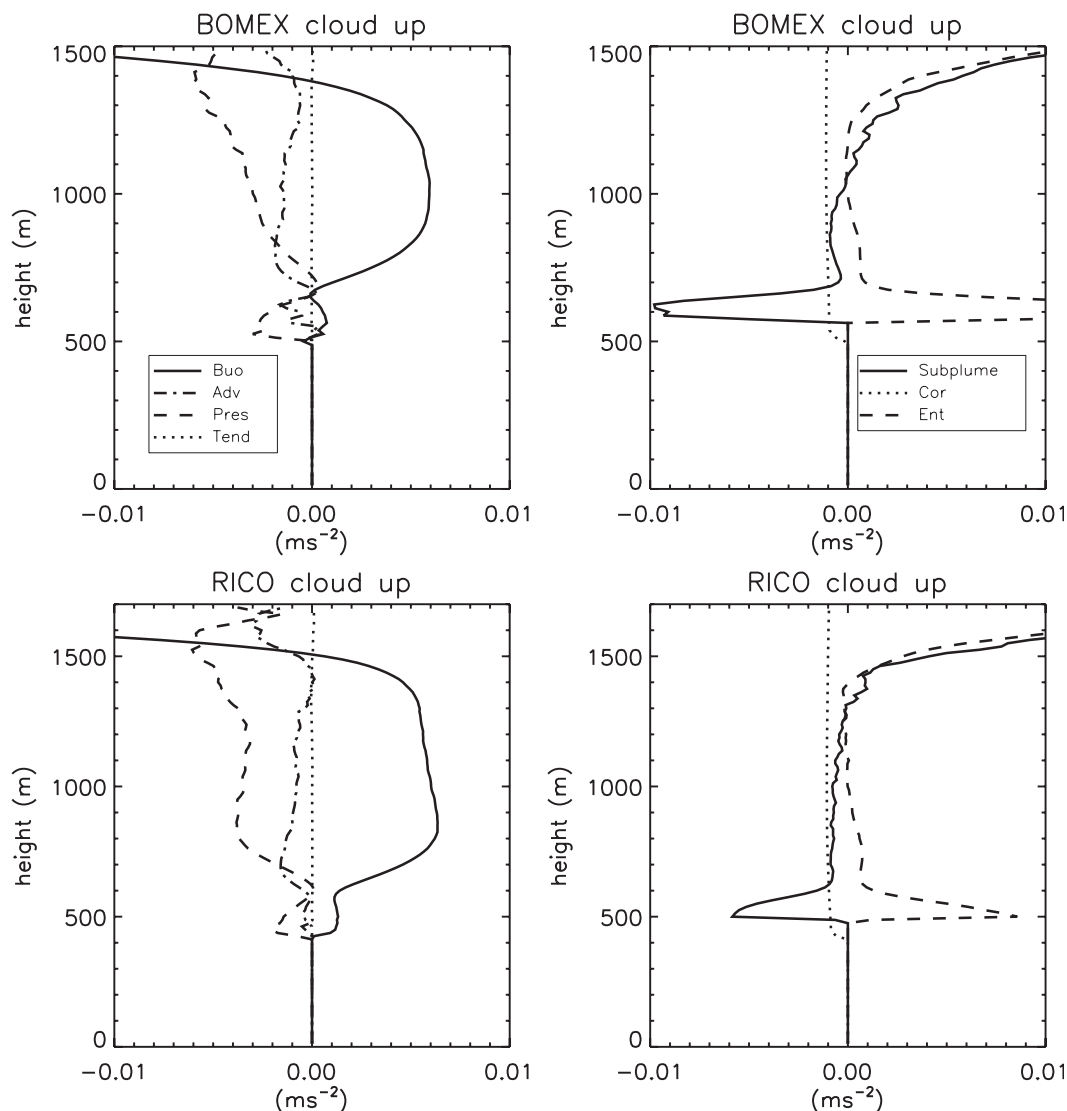
FIG. 2. Hourly-mean in-cloud vertical velocity budgets according to Eq. (5) as obtained from the 8th and 18th hours of the (top) BOMEX and (bottom) RICO simulations, respectively, for the cloud updraft decomposition. Line styles as indicated in the legend.

well defined. The most important consequence is that a parameterization for the damping of the in-cloud vertical velocity by an entrainment term seems misleading, as the pressure term is the major sink term in the in-cloud vertical velocity budget rather than the entrainment term.

4. Determination of the parameterization coefficients a and b in the in-cloud vertical velocity equation

The budget analysis has demonstrated that there is no real physical basis for the format of Eq. (1) as used by virtually all convection parameterization schemes for

large-scale models. This is largely due to the identifications of the entrainment and detrainment rates E and D with the various lateral mixing terms as given by Eq. (A7) that give different and in fact unphysical values if applied to the vertical velocity budget equation. Therefore as a pragmatic way we will proceed by using the fractional entrainment rates that are diagnosed from the budget equation from the conserved thermodynamic variables such as the total water specific humidity q_t and use this as a damping length scale in the vertical velocity equation. This is partly inspired by the fact that in convection parameterizations the same entrainment rates are used for the vertical velocity equations as for the
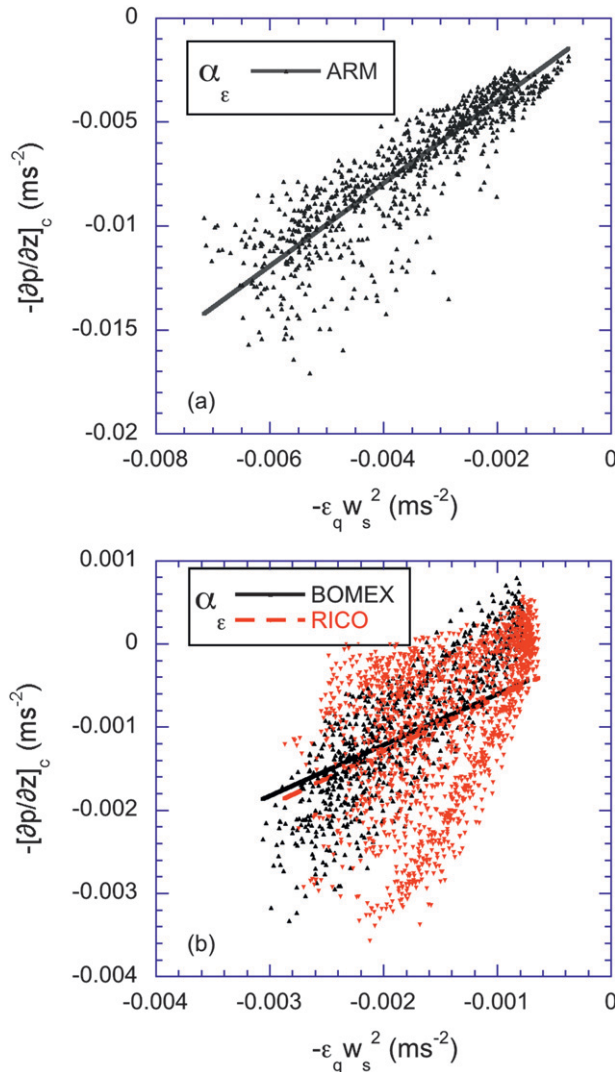
FIG. 3. Scatterplots of the lateral entrainment and the pressure gradient in cloud updrafts: (a) ARM case, and (b) BOMEX and RICO. Each data point represents a 10-min average value at an arbitrary level and arbitrary time in the cloud. The lines show a linear fit through the origin, and the values of α_ϵ are presented in Table 3.

TABLE 3. Fit coefficients α_ϵ, α_B, γ, and η of a linear regression through the origin for the scatterplots presented in Figs. 3, 4, 5, and 7.

	Cloud core			Cloud updraft		
	BOMEX	ARM	RICO	BOMEX	ARM	RICO
$-\left[\dfrac{\partial p}{\partial z}\right]_c = -\alpha_\epsilon \epsilon_q w_c^2$	1.6	3.5	1.8	0.6	2.0	0.65
$-\left[\dfrac{\partial p}{\partial z}\right]_c = \alpha_B B_c$	-0.45	-0.9	-0.5	-0.3	-0.9	-0.3
$\epsilon_q w_c^2 = \gamma B_c$	0.3	0.25	0.25	0.45	0.45	0.4
$\dfrac{1}{2}\dfrac{\partial w_c^2}{\partial z} = \eta B_c$	0.35	0.3	0.25	0.35	0.35	0.3

if there is some experimental evidence for this assumption, Fig. 3 shows scatterplots of the diagnosed pressure term versus the entrainment term for all three cases. Each data point represents a 10-min averaged value at an arbitrary level in the cloud, and was selected on the basis of three criteria—namely, a minimum value for the cloud area fraction (0.015 and 0.02 for the cloud core and cloud updraft sampling, respectively), a minimum buoyancy ($B_c > 0.001$ m s^{-2}), and a positive value for the diagnosed fractional entrainment rate ϵ_q. The figures also show a linear fit through zero. Although we can observe a reasonable correlation, the relationship varies strongly from case to case. To make that notion more quantitative, Table 3 shows the coefficients obtained from a linear fit through the origin for both the cloud updraft and the cloud core decomposition. This shows that the proportionality constant α_ϵ varies by more than a factor of 3 from case to case. As it has been also suggested in the literature that the pressure term can be scaled with the buoyancy term we also show a similar scatterplot for these terms in Fig. 4. Although the correlation is higher between these terms, Table 3 shows also here a strong variation from case to case for the proportionality constant α_B. So it seems difficult to directly incorporate the pressure gradient term into either the entrainment or the buoyancy term.

We therefore proceed by taking Eq. (1) at face value and find the best value for both a and b for all LES data points of each case separately by minimizing the cost function s:

cloudy updraft equations for heat and moisture. So, in practice, we diagnose ϵ_q from the total specific humidity q_t field following Siebesma et al. (2003):

$$\epsilon_q(z) = -\frac{\partial q_{t,c}/\partial z}{q_{t,c} - \overline{q_t}}, \qquad (7)$$

where $q_{t,c}$ indicates the conditionally sampled total specific humidity, and use this diagnosed ϵ_q in the parameterized vertical velocity Eq. (1). By using the coefficients a and b in Eq. (1), one implicitly assumes that the pressure and subplume terms are proportional to the buoyancy or the fractional entrainment term. To verify

$$s(a,b) = \sqrt{\frac{1}{N}\sum_{i=1}^{N}\left(aB_{s,i} - b\epsilon_{q,i}w_{s,i}^2 - \frac{1}{2}\frac{\partial w_{s,i}^2}{\partial z}\right)^2}, \quad (8)$$

with N the number of 10-min averaged LES data points. Figure 5 shows $s/s_{\min}$ as a function of a and b for the three cases of interest. The variable $s_{\min}$ is the minimum value for s, and is equal to 0.0004, 0.0013, and 0.0003 for the BOMEX, ARM, and RICO cases, respectively. The
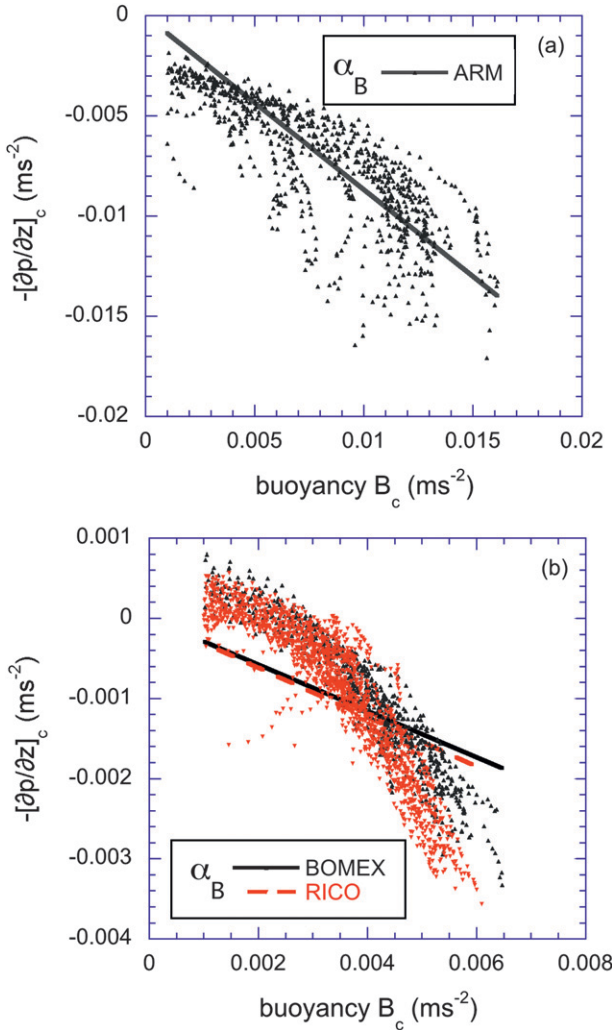
FIG. 4. Scatterplots of the buoyancy and the pressure gradient in cloud updrafts: (a) ARM case, and (b) BOMEX and RICO. Each data point represents a 10-min average value at an arbitrary level and arbitrary time in the cloud. The lines show a linear fit through the origin, and the values of α_B are presented in Table 3.

optimal solutions with minimum error for s are found for $a = 0.55$, $b = 0.45$ (BOMEX); $a = 0.35$, $b = 0.0$ (ARM); and $a = 0.45$, $b = 0.35$ (RICO). Indeed these values differ substantially from each other, but this is due to the fact that the error is not very sensitive to the precise choice of a and b. For example, the area for which $s/s_{min} < 2$ shows a narrow ellipselike structure for all three cases that largely overlap with each other. To explain this finding, let us follow (Gregory 2001), who assumed a linear relation between the entrainment and buoyancy terms:

$$\epsilon_q w_c^2 = \gamma B_c, \qquad (9)$$

with γ a proportionality constant. Figure 6 gives some support for this scaling and Table 3 provides the results

of a linear regression for γ. Although the uncertainty is quite high for γ, the variation from case to case is relatively small and amounts to $\gamma \simeq 0.4$ to 0.45—values much larger than the value $1/12$ proposed by Gregory (2001). Substitution of Eq. (9) into Eq. (1) gives

$$\frac{1}{2}\frac{\partial w_c^2}{\partial z} = (a - b\gamma)B_c \equiv \eta B_c, \qquad (10)$$

where the factor η can be interpreted as an efficiency factor that measures the fraction of CAPE that is converted into kinetic energy. This efficiency factor η can also be deduced from LES data through a linear fit of the scatter data of the buoyancy term versus the advection term such as displayed in Fig. 7. The deduced values for η are displayed in Table 3 showing an efficiency that varies from 0.30 for RICO to 0.35 for ARM and BOMEX for the cloud updraft decomposition. This is a similar efficiency factor as found in De Rooy and Siebesma (2010).

If we accept Eq. (10), it follows directly that the proportionality factors a and b are dependent variables that are related to γ and η through a straight line:

$$a = \gamma b + \eta. \qquad (11)$$

If we plot the straight lines according to Eq. (11) in Fig. 6 using the fitted values from Table 3, we indeed see a near collapse of this line with the major axis of the ellipses. So the relation in Eq. (11) can be interpreted as the set of combination of values for a and b that gives equally optimal estimates for the vertical velocity as represented by Eq. (1).

Figure 8 finally shows again the same relationships [Eq. (11)] for all three cases in Table 1. A number of conclusions can be drawn from this figure. The fact that the three lines approximately coincide reflects that the diagnosed values for η and γ for the three cases are in reasonable agreement with each other. Furthermore, three specific combinations of a and b can be highlighted. Firstly the zero crossing of the lines of the b axis corresponds to the case $(a \simeq 1/3, b = 0)$, where Eq. (1) describes a balance between the advection term and a reduced buoyancy term, which are related through the efficiency factor η. Secondly, there is the option $(a \sim 0.75, b = 1)$ in which the entrainment term is used along with a reduction factor for the buoyancy term as suggested by Bechtold et al. (2001) and De Rooy and Siebesma (2010). Finally, one can use the option where $(a = 1, b \sim 1.5)$, in which the buoyancy term is used without a reduction factor and with an enhanced damping for the entrainment term. The results of the LES runs all favor combinations of a and b that correspond to a reduction of the lateral entrainment and subsequently a strong
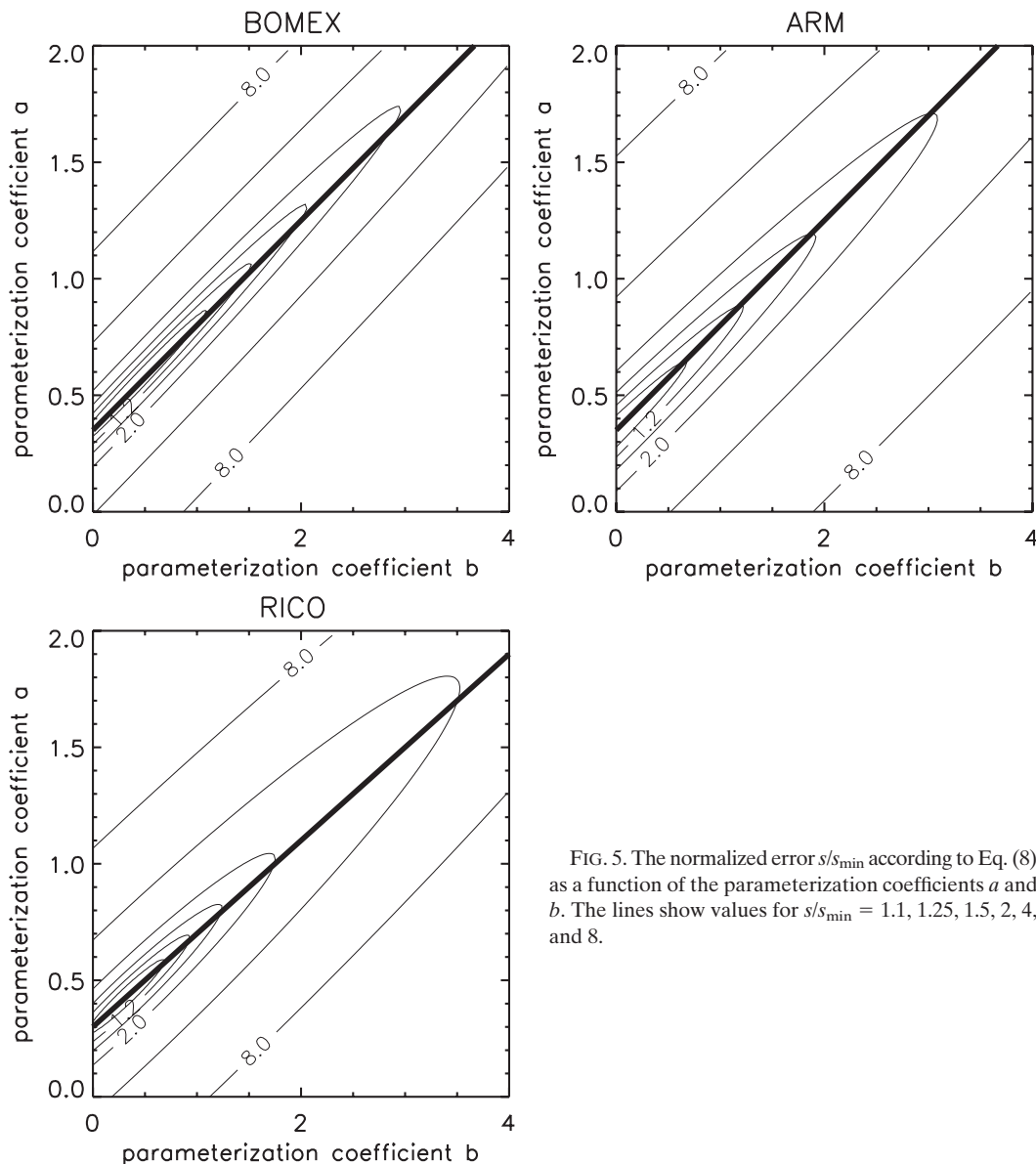
FIG. 5. The normalized error s/s_{min} according to Eq. (8) as a function of the parameterization coefficients a and b. The lines show values for $s/s_{min} = 1.1, 1.25, 1.5, 2, 4,$ and 8.

reduction of the buoyancy term. The various results from the literature as summarized in Table 1 are also displayed in Fig. 8. These results clearly show that a considerable number of these proposals should be rejected based on this analysis as they are too far from the line given by Eq. (11).

5. Conclusions and outlook

We used LES results to study the in-cloud vertical velocity budget and to diagnose the coefficients used for the parameterized vertical velocity equation. It is found that the in-cloud vertical velocity is governed by a bulk balance between production by buoyancy and

consumption by the pressure and advection terms. The fact that the pressure term is the dominant damping term is at odds with operational models that use a lateral entrainment term as the prime damping term of the vertical velocity. The values for the lateral entrainment term in the in-cloud vertical velocity budget are found to be small and even positive, which indicates negative values for the lateral entrainment rate of vertical velocity. Models that solve the in-cloud vertical velocity equation for convective clouds, however, apply the same lateral entrainment rates as used for the thermodynamic quantities, and for further study of the parameterized vertical velocity equation we consistently used the lateral entrainment as obtained from the total specific humidity
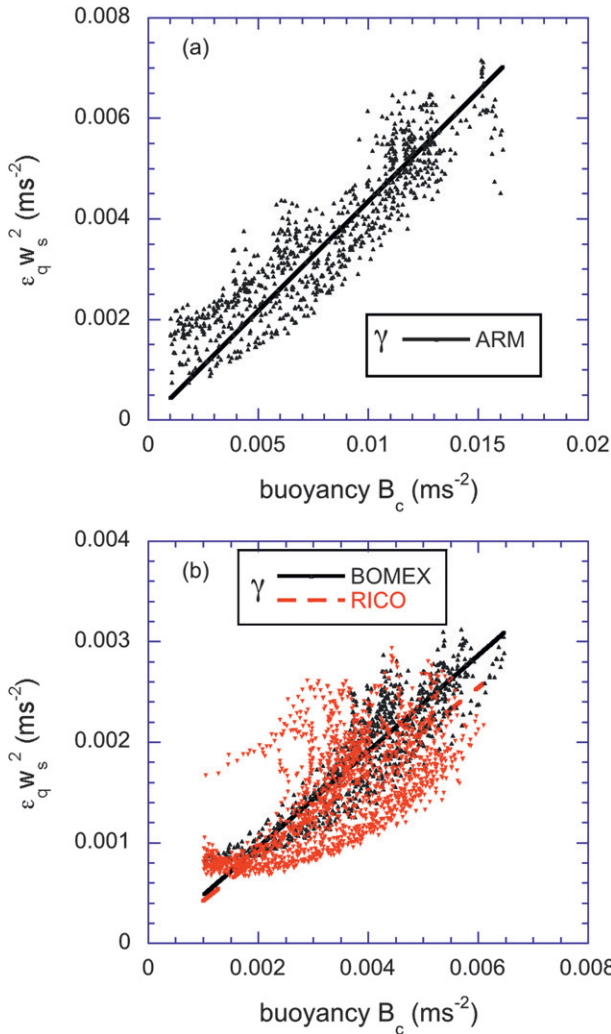
FIG. 6. Scatterplots of the buoyancy and the lateral entrainment term in cloud updrafts: (a) ARM case, and (b) BOMEX and RICO. Each data point represents a 10-min average value at an arbitrary level and arbitrary time in the cloud. The lines show a linear fit through the origin, and the values of γ are presented in Table 3.
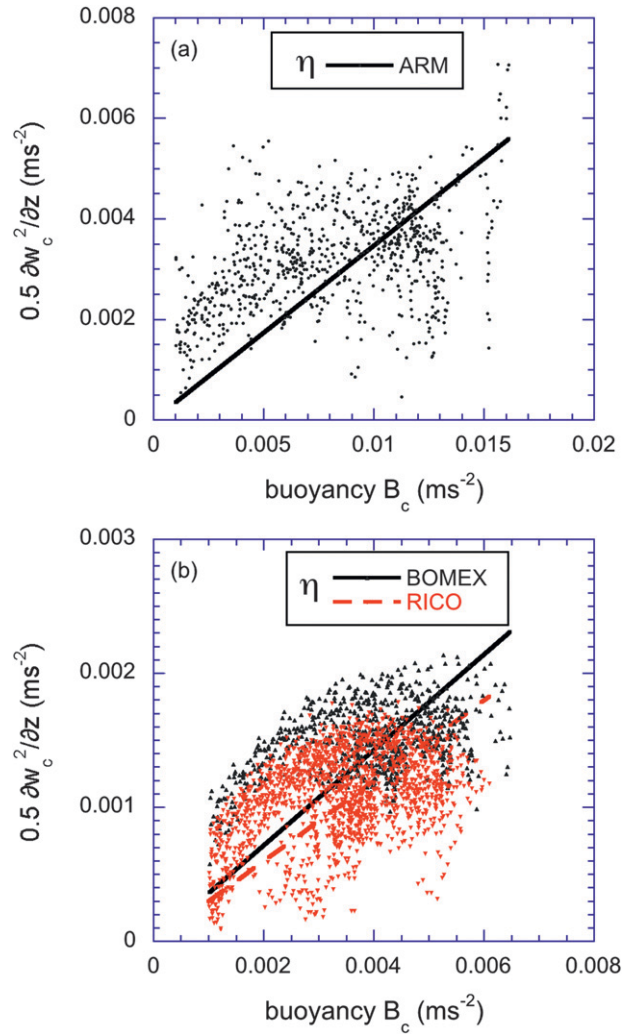
FIG. 7. Scatterplots of the buoyancy and the advection term in cloud updrafts: (a) ARM case, and (b) BOMEX and RICO. Each data point represents a 10-min average value at an arbitrary level and arbitrary time in the cloud. The lines show a linear fit through the origin, and the values of η are presented in Table 3.

fields. In this way we made an attempt to calculate optimum values for the proportionality factors a for the buoyancy and b for the lateral entrainment term. Using a least error analysis, we found $a = 0.55$, $b = 0.45$ for BOMEX; $a = 0.35$, $b = 0.0$ for ARM; and $a = 0.45$, $b = 0.35$ for RICO. The parameterization coefficients are thus case dependent. However, it is found that a rather wide range of values for a and b give relatively small errors and will yield a rather truthful representation of the advection term. It is explained that this result can be expected in case the buoyancy and the lateral entrainment term are approximately linearly related. The LES results enable to draw an important conclusion regarding the most appropriate choice for the parameterization

coefficients a and b. Setting $b = 0$ implies a balance between the advection and a reduced buoyancy. In that case the factor a should be taken equal to the efficiency factor η, which measures the fraction of CAPE that is converted into kinetic energy. For $b = 0$, the LES results suggest $a = \eta \approx 1/3$. Another possibility could be to use the actual value for the buoyancy by setting $a = 1$, for which we find $b \sim 1.5$ as a suitable value. Alternatively, one can use the actual value for the entrainment and use a reduction factor of the buoyancy of approximately $a \sim 0.75$—a combination that is close to suggestions done by various authors (De Rooy and Siebesma 2010; Bechtold et al. 2001). The other proposals that are plotted in Fig. 8 should be rejected based on the present results. One
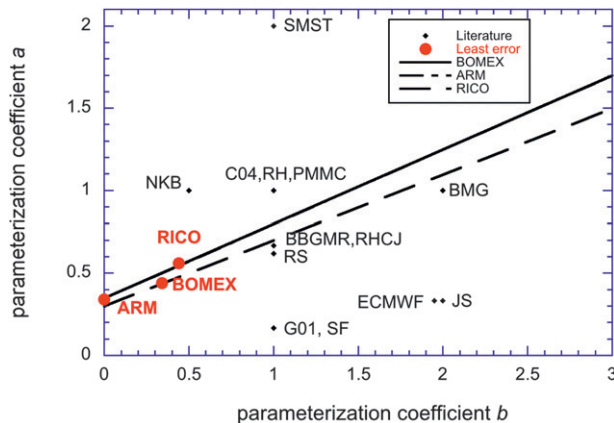
FIG. 8. Dependency of the parameterization factor b on a according to Eq. (11) following the assumption that the lateral entrainment term is linearly proportional to the buoyancy. The lines were calculated with use of the results for the cloud updraft decomposition shown in Table 3. The solid line represents the BOMEX case, and the two dashed lines indicating the ARM and RICO results fall on top of each other and cannot be distinguished individually. Also shown are the optimum values for the three cumulus cases obtained from a least error analysis and some proposed values for a and b to be used for the parameterized vertical velocity equation according to Eq. (1). The explanation of the acronyms is presented in Table 1.

should however keep in mind that these results are obtained based on entrainment rates that are deduced from a cloud updraft decomposition. If one is building a cloud model based on another decomposition (e.g., the cloud core), one does find for instance a slightly lower efficiency η of typically 0.3. Although the results show that all combinations of a and b given by Eq. (11) are acceptable, one could argue that the combination with $b = 0$ is more robust and realistic as the entrainment term in Eq. (1) is in fact a rather artificial damping term that is also introducing an extra uncertainty as one needs to come up with a realistic estimate for the fractional entrainment ϵ_q.

We have done the analyses for a limited number of (three) cases. It would be interesting to explore a more complete phase space of realizations for shallow convection to further test the robustness of the results presented here. The recent development of a version of DALES that runs on a graphical processor unit (GPU) and that shows a spectacular speedup of the numerical performance would be an excellent tool for such a further exploration (Schalkwijk et al. 2012). Finally, one last topic to possibly explore is an objective verification of the numerical solutions of the vertical velocity Eq. (1) fed by the proper initial conditions, entrainment rates, and parameterization coefficients provided by LES, and then evaluate the vertical velocity profiles for a large number of cases.

APPENDIX

The Conditionally Sampled Budget Equation for the Vertical Velocity

The LES model solves the following equation for the vertical velocity:

$$\frac{\partial w}{\partial t} = -\frac{\partial u_j w}{\partial x_j} - \frac{\partial \tau_{3j}}{\partial x_j} + \frac{g}{\theta_0}\theta_v - \frac{1}{\rho_0}\frac{\partial P}{\partial z} + 2\Omega\cos\varphi u, \quad (A1)$$

with ρ_0 a constant reference density, P the pressure, and τ_{3j} represents the subfilter contribution accounting for fluctuations at scales smaller than the filter length scale applied in the LES. A few steps have to be taken to rewrite Eq. (A1) in a form that is similar to our starting point Eq. (3). It is convenient to define the slab-mean hydrostatic pressure gradient equal to the horizontal slab-mean buoyancy:

$$\frac{1}{\rho_0}\frac{\partial \overline{p}_{\text{hyd}}}{\partial z} \equiv \frac{g}{\theta_0}\overline{\theta_v}, \qquad (A2)$$

where the overbar is used to indicate a horizontal-mean value.

Next, we introduce the modified "pressure" p:

$$p \equiv \frac{1}{\rho_0}(P - \overline{p}_{\text{hyd}}). \qquad (A3)$$

Note that the pressure P includes a fraction of the subgrid TKE in order to compensate for its inclusion in the subgrid momentum flux τ_{ij} (Deardorff 1973). Now we can eliminate the pressure P from Eq. (A1) to give

$$\frac{\partial w}{\partial t} = -\frac{\partial u_j w}{\partial x_j} - \frac{\partial \tau_{3j}}{\partial x_j} + \frac{g}{\theta_0}(\theta_v - \overline{\theta_v}) - \frac{\partial p}{\partial z} + 2\Omega\cos\varphi u.$$
$$(A4)$$

In this study we used this equation for diagnosis of the in-cloud vertical velocity budget.

Different conditional sampling criteria can be applied to clouds. For example, the cloud core decomposition, which only considers positively buoyant clouds, provides an excellent means to parameterize vertical turbulent

transport using the mass flux approach (Siebesma and Cuijpers 1995). On the other hand, for radiative transfer calculations one needs to consider the total cloud area. In any case, the conditionally sampled horizontal slab-mean value for any arbitrary scalar quantity ψ can be calculated with an indicator function I_s:

$$[\psi]_c(z,t) = \frac{\int_A I_s(x,y,z,t)\psi(x,y,z,t)\,dA}{\int_A I_s(x,y,z,t)\,dA}, \quad (A5)$$

with the indicator function $I_s = 1$ if a sampling criterion is satisfied, and $I_s = 0$ otherwise. The square brackets $[\psi]_c$ are used to indicate the conditionally sampled horizontal slab-mean value. In the remainder of the paper these square brackets are, for notational convenience, omitted except when the operator is applied to a derivative. If the sampling operator is applied to a derivative, one needs to invoke the chain rule of differentiation, in addition to Leibniz's rule (Young 1988; Schumann and Moeng 1991):

$$\left[\frac{\partial w}{\partial t}\right]_c = \frac{\partial w_c}{\partial t} + \frac{w_c}{\sigma}\frac{\partial \sigma}{\partial t} + \left\{\frac{\partial w}{\partial t}\right\}_L. \quad (A6)$$

The extra term that arises is indicated with parentheses and a subscript "L." After applying the sampling operator to Eq. (A4), taking into the account the Leibniz terms, and noting that the subfilter vertical velocity variance τ_{33} is counted as a part that contributes to the subplume vertical velocity variance, it follows from a comparison to Eq. (3) that the lateral mixing term includes the following contributions:

$$\frac{E_w}{\rho}w_e - \frac{D_w}{\rho}w_c = -\sigma\left[\frac{\partial u_h w}{\partial x_h}\right]_c - \sigma\left[\frac{\partial \tau_{3h}}{\partial x_h}\right]_c - \sigma\left\{\frac{\partial w}{\partial t}\right\}_L$$
$$- \sigma\left\{\frac{\partial ww}{\partial z}\right\}_L - \sigma\left\{\frac{\partial \tau_{33}}{\partial z}\right\}_L, \quad (A7)$$

where $h = 1, 2$ is used to denote derivatives in the horizontal directions only. With aid of the continuity equation in mass flux form [Eq. (4)], the lhs of Eq. (A7) can be expressed as

$$\frac{E_w}{\rho}w_e - \frac{D_w}{\rho}w_c = -\frac{\epsilon_w \sigma w_c^2}{1-\sigma} + w_c\frac{\partial \sigma}{\partial t} + w_c\frac{\partial M_c}{\partial z}, \quad (A8)$$

which implies that the lateral entrainment term in the conditionally sampled vertical velocity Eq. (5) is given by

$$-\frac{\epsilon_w w_c^2}{1-\sigma} = -\frac{w_c}{\sigma}\frac{\partial \sigma}{\partial t} - \frac{w_c}{\sigma}\frac{\partial M_c}{\partial z} - \left[\frac{\partial u_h w}{\partial x_h}\right]_c - \left[\frac{\partial \tau_{3h}}{\partial x_h}\right]_c$$
$$- \left\{\frac{\partial w}{\partial t}\right\}_L - \left\{\frac{\partial ww}{\partial z}\right\}_L - \left\{\frac{\partial \tau_{33}}{\partial z}\right\}_L. \quad (A9)$$

In addition to the horizontal flux of resolved and subgrid vertical momentum across the cloud boundaries, the lateral mixing term also includes terms that arise from the Leibniz rule. For example, some air parcels that are vertically accelerated may disappear from the cloud ensemble at the next time step, which is counted as lateral mixing of momentum.

REFERENCES

Arakawa, A., and W. H. Schubert, 1974: Interaction of a cumulus cloud ensemble with the large-scale environment: Part I. *J. Atmos. Sci.,* **31,** 674–701.

Bechtold, P., E. Bazile, F. Guichard, P. Mascart, and E. Richard, 2001: A mass-flux convection scheme for regional and global models. *Quart. J. Roy. Meteor. Soc.,* **127,** 869–886.

Bretherton, C. S., J. R. McCaa, and H. Grenier, 2004: A new parameterization for shallow cumulus convection and its application to marine subtropical cloud-topped boundary layers. Part I: Description and 1D results. *Mon. Wea. Rev.,* **132,** 864–882.

Brown, A. R., and Coauthors, 2002: Large-eddy simulation of the diurnal cycle of shallow cumulus convection over land. *Quart. J. Roy. Meteor. Soc.,* **128,** 1075–1093.

Cheinet, S., 2004: A multiple mass-flux parameterization for the surface-generated convection. Part II: Cloudy cores. *J. Atmos. Sci.,* **61,** 1093–1113.

Dawe, J. T., and P. H. Austin, 2011a: The influence of the cloud shell on tracer budget measurements of LES cloud entrainment. *J. Atmos. Sci.,* **68,** 2909–2920.

——, and ——, 2011b: Interpolation of LES cloud surfaces for use in direct calculations of entrainment and detrainment. *Mon. Wea. Rev.,* **139,** 444–456.

Deardorff, J. W., 1973: Three-dimensional numerical modeling of the planetary boundary layer. *Workshop on Micrometeorology,* D. A. Haugen, Ed., Amer. Meteor. Soc., 271–311.

De Rooy, W. C., and A. P. Siebesma, 2010: Analytical expressions for entrainment and detrainment in cumulus convection. *Quart. J. Roy. Meteor. Soc.,* **136,** 1216–1227.

ECMWF, 2010: IFS documentation—Cy36r1: Operational implementation 26 January 2010. Part IV: Physical processes, European Centre for Medium-Range Weather Forecasts Tech. Rep., 171 pp.

Golaz, J.-C., M. Salzmann, L. J. Donner, L. W. Horowitz, Y. Ming, and M. Zhao, 2011: Sensitivity of the aerosol indirect effect to subgrid variability in the cloud parameterization of the GFDL atmosphere general circulation model AM3. *J. Climate,* **24,** 3145–3160.

Grant, A. L. M., 2001: Cloud-base fluxes in the cumulus-capped boundary layer. *Quart. J. Roy. Meteor. Soc.,* **127,** 407–421.

Gregory, D., 2001: Estimation of entrainment rate in simple models of convective clouds. *Quart. J. Roy. Meteor. Soc.,* **127,** 53–72.

Heus, T., and H. J. J. Jonker, 2008: Subsiding shell around shallow cumulus clouds. *J. Atmos. Sci.,* **65,** 1003–1018.

——, and Coauthors, 2010: Formulation of the Dutch Atmospheric Large-Eddy Simulation (DALES) and overview of its applications. *Geosci. Model Dev.,* **3,** 415–444, doi:10.5194/gmd-3-415-2010.

Jakob, C., and A. P. Siebesma, 2003: A new subcloud model for mass-flux convection schemes: Influence on triggering, updraft properties, and model climate. *Mon. Wea. Rev.,* **131,** 2765–2778.

Jonker, H. J. J., T. Heus, and P. P. Sullivan, 2008: A refined view of vertical mass transport by cumulus convection. *Geophys. Res. Lett.,* **35,** L07810, doi:10.1029/2007GL032606.

Kim, D., and I.-S. Kang, 2011: A bulk mass flux convection scheme for climate model: Description and moisture sensitivity. *Climate Dyn.,* **38,** 411–429, doi:10.1007/s00382-010-0972-2.

Neggers, R. A. J., M. Koehler, and A. C. M. Beljaars, 2009: A dual mass flux framework for boundary layer convection. Part I: Transport. *J. Atmos. Sci.,* **66,** 1465–1487.

Pergaud, J., V. Masson, S. Malardel, and F. Couvreux, 2009: A parameterization of dry thermals and shallow cumuli for mesoscale numerical weather prediction. *Bound.-Layer Meteor.,* **132,** 83–106, doi:10.1007/s10546-009-9388-0.

Rio, C., and F. Hourdin, 2008: A thermal plume model for the convective boundary layer: Representation of cumulus clouds. *J. Atmos. Sci.,* **65,** 407–425.

——, ——, F. Couvreux, and A. Jam, 2010: Resolved versus parametrized boundary-layer plumes. Part II: Continuous formulations of mixing rates for mass-flux schemes. *Bound.-Layer Meteor.,* **135,** 469–483.

Romps, D. M., 2010: A direct measure of entrainment. *J. Atmos. Sci.,* **67,** 1908–1927.

Schalkwijk, J., E. R. Griffith, F. H. Post, and H. J. J. Jonker, 2012: High-performance simulations of turbulent clouds on a desktop PC: Exploiting the GPU. *Bull. Amer. Meteor. Soc.,* **93,** 307–314.

Schumann, U., and C.-H. Moeng, 1991: Plume budgets in clear and cloudy convective boundary layers. *J. Atmos. Sci.,* **48,** 1758–1770.

Siebesma, A. P., and J. W. M. Cuijpers, 1995: Evaluation of parametric assumptions for shallow cumulus convection. *J. Atmos. Sci.,* **52,** 650–666.

——, and Coauthors, 2003: A large eddy simulation intercomparison study of shallow cumulus convection. *J. Atmos. Sci.,* **60,** 1201–1219.

——, P. M. M. Soares, and J. Teixeira, 2007: A combined eddy-diffusivity mass-flux approach for the convective boundary layer. *J. Atmos. Sci.,* **64,** 1230–1248.

Simpson, J., and V. Wiggert, 1969: Models of precipitating cumulus towers. *Mon. Wea. Rev.,* **97,** 471–489.

Soares, P. M. M., P. M. A. Miranda, A. P. Siebesma, and J. Teixeira, 2004: An eddy-diffusivity/mass-flux approach for dry and shallow cumulus convection. *Quart. J. Roy. Meteor. Soc.,* **130,** 3365–3384.

Tiedtke, M., 1989: A comprehensive mass flux scheme for cumulus parameterization in large-scale models. *Mon. Wea. Rev.,* **117,** 1779–1800.

VanZanten, M. C., and Coauthors, 2011: Controls on precipitation and cloudiness in simulations of trade-wind cumulus as observed during RICO. *J. Adv. Model. Earth Syst.,* **3,** M06001, doi:10.1029/2011MS000056.

Von Salzen, K., and N. A. McFarlane, 2002: Parameterization of the bulk effects of lateral and cloud-top entrainment in transient shallow cumulus clouds. *J. Atmos. Sci.,* **59,** 1405–1430.

Young, G. S., 1988: Turbulence structure of the convective boundary layer. Part III: The vertical velocity budgets of thermals and their environment. *J. Atmos. Sci.,* **45,** 2039–2049.